A New Resonant Fault Current Limiter for Improved Wind Turbine Transient Stability

Slava Demin, Moshe Sitbon, Ilan Aharon, Eli Barbi, Ram Machlev, Juri Belikov, Yoash Levron, and Dmitry Baimel

***Abstract*— This paper proposes a new resonance-type FCL, which is designed specifically for DFIG-based wind turbines. The proposed topology overcomes the well-documented drawbacks associated with conventional resonance-based FCLs while preserving the advantages of this topology. The proposed circuit limits the fault current for the entire fault period independently of the reactor's charging state and significantly reduces the wind turbine's torque oscillations during a fault. The proposed FCL is simulated as part of a power system that includes a wind turbine, synchronous generator, and two step-up transformers. The results show that during a three-phase to-ground fault, the proposed FCL significantly improves the system's stability, and leads to improved fault current, voltage, active power, reactive power, and torque transients.**

***Keywords*: Fault current limiter, FCL, transient stability, DFIG, resonance.**

I. Introduction

WIND turbines are the second largest supplier of renewable energy after hydropower plants. The capacity of wind power generation is constantly increasing worldwide and in total, 466 GW of onshore wind turbines are expected to be built in 2022-2026. The offshore market is expected to grow from 21.1 GW in 2021 to 31.4 GW in 2026. It is also expected that by the year 2050, wind turbines will provide more than 8,000 GW worldwide, generating more electricity than any other energy source [1]. Furthermore, between the years 2010-2019, the price of kWh for onshore wind generation decreased by 40%, and for offshore generation by 30% [2].

Implementation of doubly-fed induction generators (DFIG) has become very popular in wind turbines with rated power below 6.5 MW and less popular in ultra-large wind turbines, with rated power higher than 8 MW, due to high maintenance cost [3]. The DFIG technology has important advantages when compared to other fixed-speed machines, such as accurate speed control and four-quadrant active and reactive power regulation. Moreover, the associated stator and rotor power converters require only 20–30% of the machine's power rating while the rotor speed is maintained in the range of 75%-125% of the nominal speed [4]. This leads to improving the ability to better harvest wind energy and lower stator power losses due to a 30% lower stator current than in permanent magnet generators (PMG). The drawback of the DFIG generators is a 40% higher failure rate than PMG [5]. However, DFIG-based turbines are vulnerable to grid faults, which lead to over-currents and voltage fluctuations, as their stators are directly linked to the grid [2]. Therefore, DFIG-based power plants have to be protected to avoid damage and prevent unnecessary downtime.

The Fault Current Limiter (FCL) must be carefully selected to protect the DFIG system. A good FCL selection will limit the fault current, enhance the fault ride-through capabilities of the DFIG wind turbine, and improve the transient stability of the whole power system. FCLs work by adding a high impedance in series to the fault path, thus keeping the fault current below a predefined limit, and preventing damage to the system. During normal operation, the FCL's impedance is kept very low to prevent voltage drop and minimize power losses [6]. At the beginning of the fault, the FCL circuit increases the value of the series impedance to limit the fault current near its nominal values [7]. As a result, FCLs allow to keep a system connected to the grid during fault for longer periods, thus improving fault ride-through (FRT) capability by reducing downtime and preventing unnecessary shutdowns [8]. In addition, the fault currents in a power system cause voltage sags and swells, power interruption, torque oscillations, increased reactive power demand, and thermal stress on the equipment. Therefore, parameters such as voltages, currents, active and reactive power, and torque are used for the evaluation of the efficiency and quality of the protection methods [9-11].

Generally, FCLs can be sorted into two main categories: superconducting [12-13] and non-superconducting [14]. The advantage of superconducting FCLs is nearly zero power losses, while its drawbacks are complex maintenance, high price, large dimensions, and weight. The advantages and disadvantages of non-superconducting are opposite to superconducting FCLs. Among the standard configurations of superconducting FCLs are resistive [15-16], inductive [17], superconducting magnetic energy storage (SMES) [18], and bridge-type FCL [19-20]. The common topologies of non-superconducting FCLs are resistive such as series dynamic braking resistor (SDBR) [21], bridge-type FCLs [22], and resonance-type FCLs [23-29].

Resonance-type FCLs limit the fault current by using different configurations of series or parallel connected LC components operating in resonance conditions at the network frequency. For example, parallel resonance (PR-FCL) FCLs create a path with high current limitation capability and benefit from exceptional economic value compared to traditional FCLs [23-26]. No expensive superconducting inductors are required. However, the main drawback of this topology is large oscillations between the inductor and capacitor during the

Slava Demin, Eli Barbi and Dmitry Baimel are with Shamoon College of Engineering, Department of Electrical and Electronics Engineering, Israel (e-mail of corresponding author: dmitrba@sce.ac.il). Moshe Sitbon and Ilan Aharon are with Ariel University, Department of and Electronics Engineering, Israel. Ram Machlev and Yoash Levron are with Technion Israel Institute of Technology, The Andrew and Erna Viterbi Faculty of Electrical and Computer Engineering, Israel. Juri Belikov is with Tallin University of Technology, Department of Software Science, Estonia.

transients under fault conditions. These oscillations may cause damage to the system. The series resonance FCL topology (SR-FCL) has a simple and cheap structure [27-29]. However, during a fault, the inductor reduces the fault current only during the first cycles until it is charged. Therefore, the main drawback of the series resonance configuration is that the fault current will not be limited when the reactor is fully charged. The series-parallel resonance FCL (SPR-FCL) can limit the fault current during the entire fault period, thus providing better transient stability of current, voltage, power, and torque, in comparison to series or parallel resonance FCLs [30-31]. Among bridge-type FCLs, the most basic topology (B-FCL) consists of a diode bridge and an inside reactor [32]. This topology has a simple structure and does not require a controller. The main disadvantage of this topology is that the fault current will be limited only for several cycles of the fault current until the limiting reactor is fully charged. Another very popular solid-state bridge topology is comprised of a diode bridge with a bypassed limiting resistor (SS-FCL) [32]. The advantage of this topology is the ability to control the value of the limited current.

This paper proposes a new resonance-type FCL topology that is based on the series resonance FCL. The proposed topology overcomes the previously mentioned drawbacks associated with conventional resonance-based FCLs while preserving the advantages of this topology. Like SS-FCL, the proposed FCL can control the value of the limited current. The proposed FCL limits the fault current for the entire fault period independently of the reactor's charging state and significantly reduces the wind turbine's torque oscillations during a fault. Additional advantages of the proposed FCL are better suppression of fault current and DC-link voltage spikes, and torque sags in comparison to series, parallel, series-parallel resonance, B-FCL and SS-FCL circuits.

The proposed FCL was compared to the conventional parallel, series, series-parallel resonance, conventional bridge, and solid-state FCLs. The comparison was conducted using a power system comprised of a 1.5 MW DFIG wind turbine, a 50MW synchronous generator, and two step-up transformers. The rest of the paper is organized as follows. Section II explains the operation principle of conventional parallel, series, and series-parallel resonance FCLs. Section III presents the proposed FCL. Simulation results are presented and discussed in section IV. The discussion of the obtained simulation results is conducted in Section V. The paper is concluded in section VI.

II. Operation Principle of Conventional Parallel and Series Resonance FCLs

A. Conventional parallel resonance FCL

The conventional parallel resonance fault current limiter is shown in Fig. 1. It is composed of two main components: a diode rectifier bridge with a switched reactor *Ldc* inside and a resonance part comprised of a parallel LC resonance circuit (*Lpr* and *Cpr*).

During normal operation of the power system, the switch T1 is turned on and nominal current flows through the dc reactor *Ldc*. This reactor is charged to the maximal value of the line current and maintains it as DC.

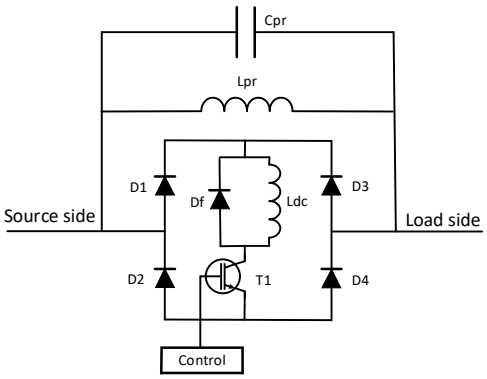

Fig. 1. Conventional parallel resonance FCL.

When the controller detects the fault current, it turns off the switch T1. The dc reactor limits the fault current during the first moments of fault occurrence until the control system will respond and turn off the switch. Opening the switch forces the current flow through the parallel resonance branch with a high impedance that limits the fault current.

B. Conventional series resonance FCL

The standard series resonance FCL scheme is shown in Fig. 2. Under normal operation, the bi-directional switch is in an off state so that inductor *Lsr* and capacitor *Csr* form a series resonance at the grid's frequency, resulting in almost zero impedance of the series path. Therefore, normal current flows through this path without power losses.

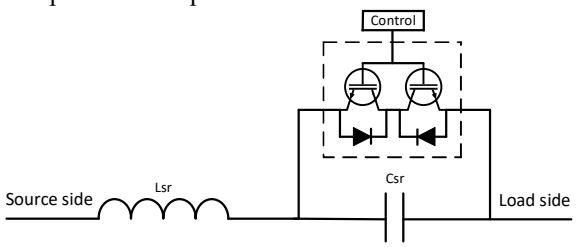

Fig. 2. Conventional series resonance FCL.

When the fault is detected, the controller turns on the switch that bypasses the capacitor *Csr*. As a result, the circuit does not remain in a resonance condition, and the FCL's impedance increases and limits the fault current.

C. Series-parallel resonance FCL

Series-parallel resonance fault current limiter has two parallel branches, as shown in Fig. 3. The first branch comprised of a reactor *Lsr*, capacitor *Csr*, and a pair of transistors, constitute the series resonance part of the circuit. The second branch consists of capacitor *Cpr* and resistor *Rpr*.

Under normal operation conditions, reactor *Lsr* and capacitor *Csr* are in series resonance at network frequency and semiconductor switches T1 and T2 are in off mode. Therefore, the total impedance of the series resonance branch is almost zero and this branch has negligible voltage drop and power losses. The capacitor *Cpr* and resistor *Rpr* have high impedance and are connected in parallel to the series resonance branch. Consequently, the line current flows through the series resonance branch.

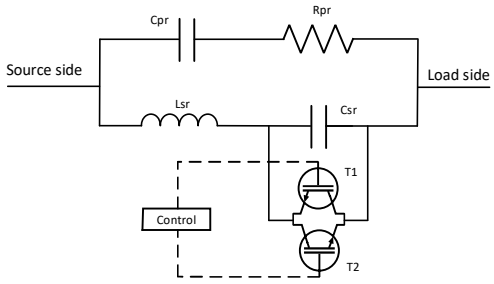

Fig. 3. Series-parallel resonance FCL.

When the fault current is detected, the controller turns on the switches T1 and T2 and bypasses the capacitor *Csr*. As a result, there is no longer series resonance and the parallel resonance branch assures connection of high impedance to the faulted line.

III. PROPOSED RESONANT FCL TOPOLOGY

The proposed FCL based on a series LC resonance circuit is shown in Fig. 4. The series-connected inductor *Lsr*, capacitor *Csr,* and the bi-directional switch T1 are in parallel to the shunt resistor *Rsh*. The values of the inductor and capacitor are chosen to be in series resonance at the network frequency according to (1), while the shunt resistor has a relatively high resistance value.

$$L_{sr} = \frac{1}{(2\pi f)^2 C_{sr}} \tag{1}$$

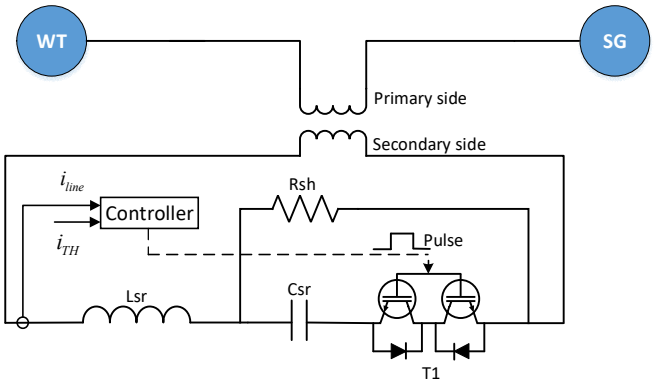

Fig. 4. The proposed resonant FCL topology.

During normal operation, the switch is turned on. Due to the series resonance, the impedance and power losses of the inductor-capacitor branch are almost zero. The shunt resistor does not have any influence on this current due to its relatively high resistance value. The FCL during normal operation has a line impedance defined by $Z_{Line} = R_{Line} + jX_{Line}$ and load impedance defined by $Z_{Load} = R_{Load} + jX_{Load}$. The sinusoidal voltage is defined by $V_s(t) = \sqrt{2}V(sin\omega t)$.

The total impedance of the FCL during normal operation is defined by

$$Z_{nrm} = R_{line} + R_{Load} + j(X_{line} + X_{Load}), \tag{2}$$

while its modulus and angle are given by

$$|Z_{nrm}| = \sqrt{(R_{line} + R_{Load})^2 + (X_{line} + X_{Load})^2}, \tag{3}$$

and

$$\theta_{nrm} = tan^{-1}\frac{2\pi f(L_{line}+L_{Load})}{R_{line}+R_{Load}}. \tag{4}$$

The voltage equation of this circuit obtained by KVL is given by

$$V_S = (R_{line} + R_{Load})i_{line} + (L_{line} + L_{Load})\frac{di_{line}}{dt} + 2V_{TF}. \tag{5}$$

where V_{TF} is the voltage drop across IGBTs.

The line current during normal operation mode is calculated by solving (5)

$$i_{line}(t) = e^{\frac{-(R_{line}+R_{Load})}{L_{line}+L_{Load}}(t-t_0)}[i_{line(I.C.)} - \frac{\sqrt{2}V}{|Z_{nrm}|}\sin(2\pi ft_0 - \theta_{nrm}) + \\ + \frac{2V_{TF}}{R_{line}+R_{Load}}] + \frac{\sqrt{2}V}{|Z_{nrm}|}\sin(2\pi ft - \theta_{nrm}) - \frac{2V_{TF}}{R_{line}+R_{Load}}, \tag{6}$$

where $i_{line(I.C.)}$ is the initial condition of the normal line current and t_0 is the time at which the line current starts flowing.

During normal operation mode, the line current is kept around its nominal value or below it. When the fault starts, the rising rate of the current is very high so the current gains dangerous values very quickly. To avoid this, FCL must identify a fault and start limiting the fault current as soon as possible. This is achieved by setting the current threshold value i_{TH} above the line current's nominal value but close to it. The fault is identified by the controller when the line current i_{line} exceeds the predefined threshold value. During the fault, the controller identifies the passing of the line current above the predefined threshold value and opens the switch to limit the fault current. However, the controller and switch have response times during which significant damage can be caused to the power system. During this response time, the rising rate of the fault current is limited by the reactor *Lsr* until the controller opens the switch T1. After opening the switch, the fault current is forced through the high-impedance path of *Lsr* and *Rsh* which limit the fault current. The shunt resistor *Rsh* has a dual purpose in the system: it increases total impedance during fault operation and has a smoothening effect on the resonance part during the transient states from normal to fault operation and vice versa. This allows for avoiding undesirable voltage oscillations, which negatively influence the power system's stability.

The total impedance of the FCL during fault operation is defined by

$$Z_F = R_{line} + R_{sh} + j(X_{line} + jX_{L_{sr}}) + \\ + \frac{(R_{Fault} + jX_{Fault})(R_{Load} + jX_{Load})}{(R_{Fault} + R_{Load}) + j(X_{Fault} + jX_{Load})} = R_F + jX_F, \tag{7}$$

while its modulus and angle are given by

$$|Z_F| = \sqrt{R_F{}^2 + X_F{}^2} \tag{8}$$

and

$$\theta_F = arctan\frac{X_F}{R_F}. \tag{9}$$

The voltage equation of the proposed FCL during fault operation is given by

$$V_S = R_F i_{line} + \frac{X_F}{2\pi f}\frac{di_{line}}{dt} + 2V_{TF}. \tag{10}$$

The fault current is given by

$$i_{Line\_F}(t) = e^{-\frac{R_F}{X_F/2\pi f}(t-t_1)}[i_{Line\_F(I.C.)} - \frac{\sqrt{2}V\sin(2\pi f t_1 - \theta_F)}{|Z_F|} + \\ + \frac{2V_{TF}}{R_F}] + \frac{\sqrt{2}V_m\sin(2\pi f t - \theta_F)}{|Z_F|} - \frac{2V_{TF}}{R_F}. \quad (11)$$

where $i_{Line\_F(I.C.)}$ is the initial condition of the fault current and t_1 is the time at which the line current starts flowing.

IV. Simulation Results

The studied power system that is shown in Fig. 5 consists of a 1.5MW DFIG wind turbine and 50MW synchronous generator that feeds 200KVA load through two step-up transformers, at a voltage of 25KV. The distances of the synchronous generator and a wind turbine from PCC are 30km and 2km, respectively.

This power system was simulated in Simulink for all compared FCLs. The simulation type is "variable-step" with a discrete solver that adjusts the simulation step size to keep pace with the actual rate of discrete state changes in the model. This adjustment can avoid unnecessary steps and shorten simulation time. The discrete solver relies on each block in the model to update its discrete states. Actually, in this simulation, Simulink models the simulated circuit by solving time domain differential equations. The step time of the simulation is set to 3μs, the time tolerance to 2.84e-13s, and the number of consecutive zero crossings to 1000. The DFIG wind turbine, transformers, generator, transmission lines, circuit breaker, load, and fault were implemented by existing Simulink blocks. However, FCLs were constructed from separate elements such as inductors, capacitors, resistors, diodes, and IGBTs.

The purpose of the simulations was to study how the proposed resonance FCL improves the transient stability of the tested power system in comparison to conventional parallel, series, series-parallel resonance, conventional bridge, and bridge solid-state FCLs. All tested FCLs are non-superconducting and their reactors have internal resistance. The tested FCLs were installed at the output of the wind turbine, after the step-up transformer. The parameters of the simulated power system are shown in Table I.

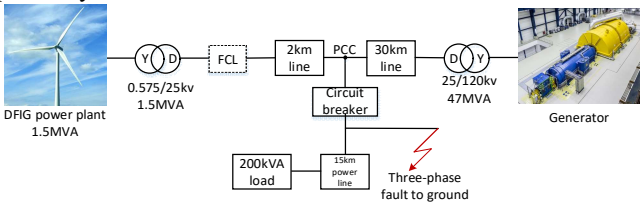

Fig. 5. The studied power system.

The proposed FCL's design parameters are values of series-connected inductor *Lsr*, capacitor *Csr,* and shunt resistor *Rsh*. The first step of the design process is to set the values of the shunt resistor *Rsh* and the inductor *Lsr* for the fault operation mode. To limit the fault current exactly to the desired and acceptable values that will ensure the safe operation of the DFIG wind turbine and protected power line, the values of *Rsh* and *Lsr* are calculated using (11). In this simulation, we aimed to limit the fault current to 1.23pu. This was achieved by *Rsh=0.48pu* and *Lsr=0.063pu.*

In the second step of the design process, the value of capacitor *Csr* is calculated. The capacitor is used only during normal operation. To ensure zero power losses during normal operation, inductor *Lsr* and capacitor *Csr* must be in resonance according to (1). We used the previously calculated value of *Lsr* to calculate the value of *Csr=0.064pu.*

TABLE I.
PARAMETERS OF THE DFIG WIND TURBINE, DC BUS, AND COMPARED FCLS.

Parameters	Value	Units
DFIG wind turbine		
Nominal mechanical output power	1.5	MW
Stator nominal voltage	575	V
Frequency	60	Hz
Stator leakage resistance	0.023	pu
Stator leakage inductance	0.18	pu
Rotor leakage resistance	0.016	pu
Rotor leakage inductance	0.16	pu
Magnetizing inductance	2.9	pu
Inertia constant	0.685	–
Friction factor	0.1	–
Pole pairs	3	–
DC bus		
Nominal DC bus voltage	1150	V
DC bus capacitor	0.01	F
FCLs		
Inductors *Ldc, Lpr, Lsr*	0.063	pu
Parallel resistor *Rpr*	0.048	pu
Series resistance *Rs* and shunt *Rsh*	0.48	pu
Series capacitor *Csr* and shunt/parallel *Csh/ Cpr*	0.064	pu
Threshold current value for turning IGBT Off	1.07	pu
Threshold current value for turning IGBT On	0.84	pu
Fault to ground resistance	0.0002	pu

The transient stability of the wind turbine was studied in terms of fault current and voltage sags limitation, active and reactive power, and torque stabilization. The performance of the compared topologies was analyzed for a three-phase to-ground fault. The fault was located close to PCC, after the circuit breaker, as shown in Fig. 5. The transient stability analysis was performed for the fault and return to normal operation periods. The fault starts at 0.25s and ends when the circuit breaker is tripped at 0.31s. Therefore, the fault period is defined as $T_{FP} \in (0.25\text{s}, 0.31\text{s})$ while the return to normal operation period is defined as $T_{RP} \in (0.31\text{s}, 0.4\text{s})$.

The transient stability evaluation index was used for the numerical evaluation of the transient stability of each studied parameter, and its definition is given by

$$E_{index} = \int_{t_{PS}}^{t_{PE}} |\Delta X| dt, \quad (11)$$

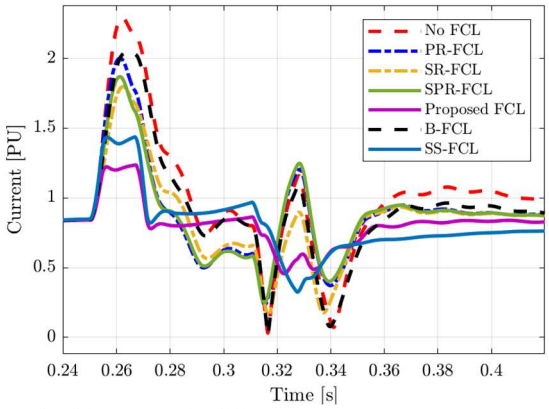

Fig. 6. Wind turbine current for different FCLs.

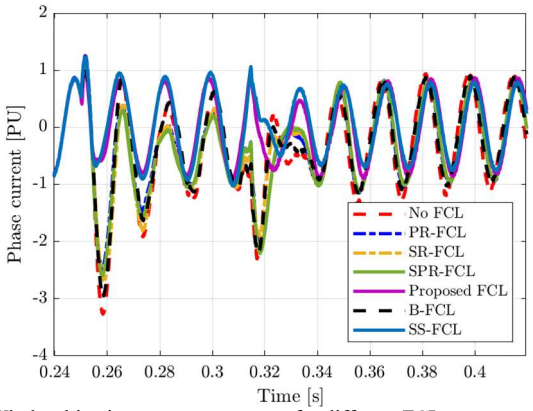

Fig. 7. Wind turbine instantaneous current for different FCLs.

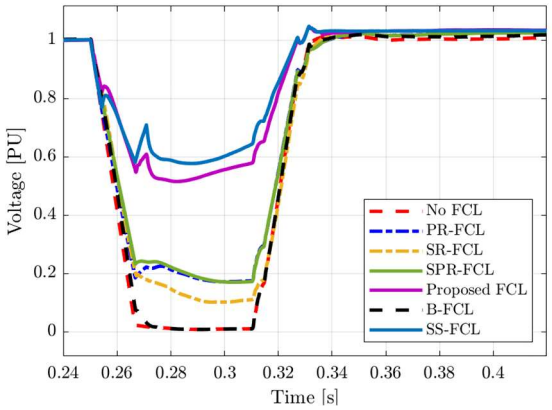

Fig. 8. Wind turbine voltage for different FCLs.

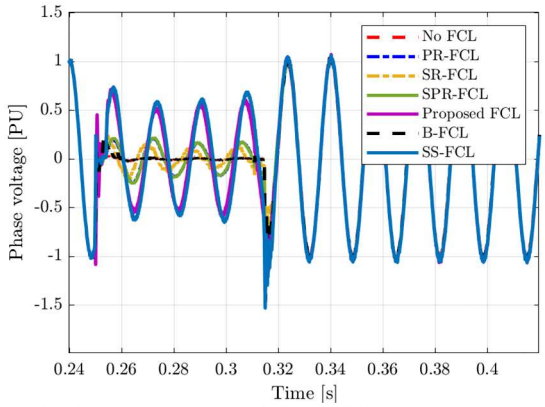

Fig. 9. Wind turbine instantaneous voltage for different FCLs.

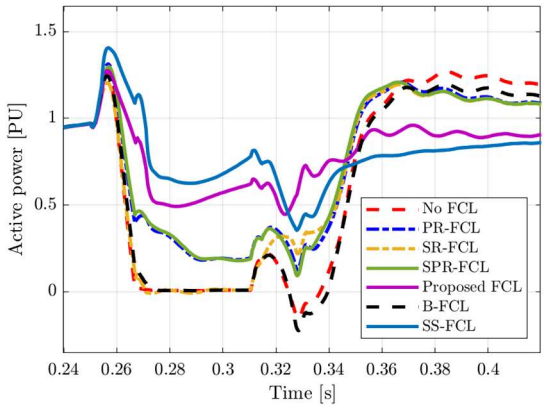

Fig. 10. Wind turbine active power for different FCLs.

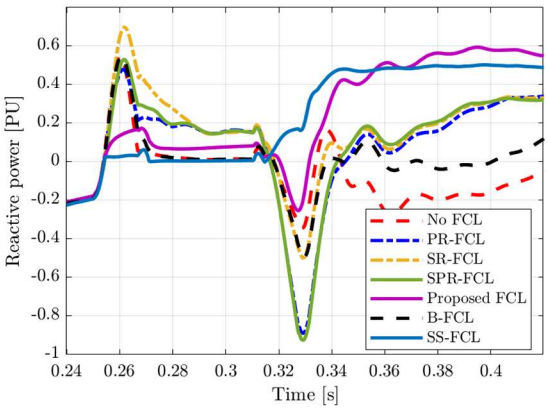

Fig. 11. Wind turbine reactive power for different FCLs.

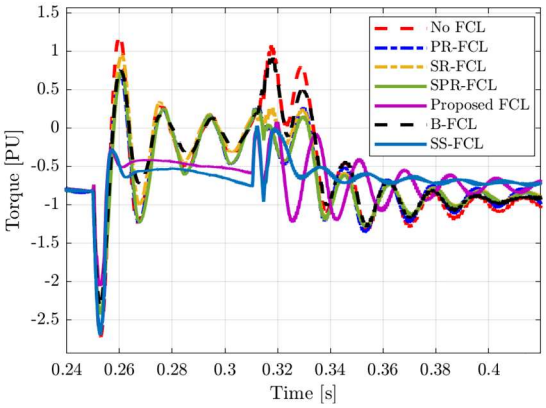

Fig. 12. Wind turbine torque for different FCLs.

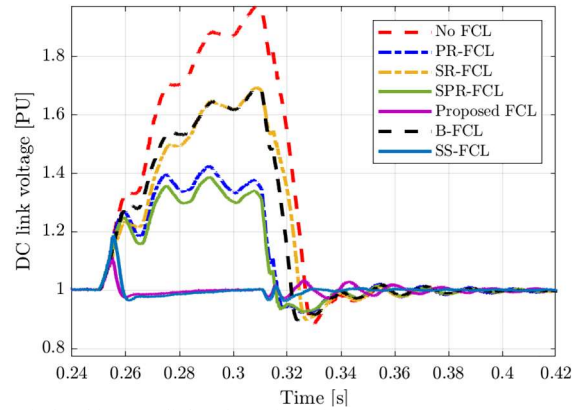

Fig. 13. Wind turbine DC-link voltage for different FCLs.

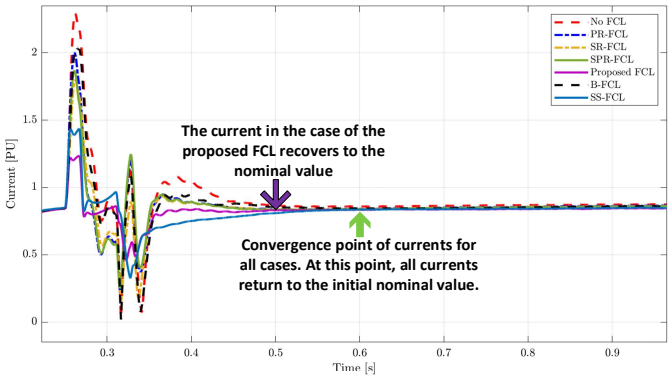

Fig. 14. Wind turbine current for different FCLs- zoom out.

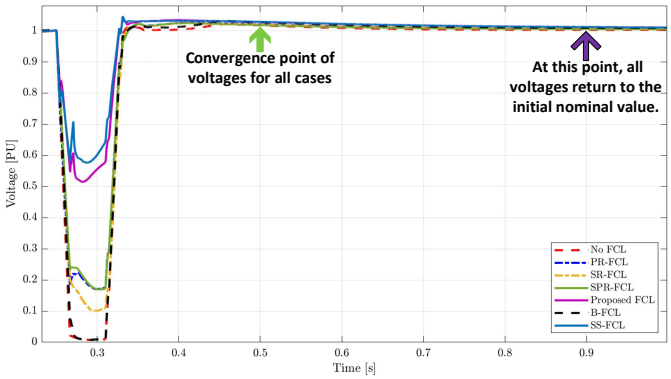

Fig. 15. Wind turbine voltage for different FCLs- Zoom out.

TABLE II.
TRANSIENT STABILITY INDEXES OF WIND TURBINE CURRENT, VOLTAGE, ACTIVE AND REACTIVE POWERS, AND TORQUE FOR ALL STUDIED CASES.

Parameters	Period	No FCL	SR-FCL	PR-FCL	SPR-FCL	Bridge-FCL	SS-FCL	Proposed FCL
Current	Fault	3.04	2.15	2.44	2.20	2.49	1.17	0.718
	Return	1.69	1.49	1.35	1.34	1.66	1.35	1.07
Voltage	Fault	5.10	4.41	4.21	4.11	5.00	2.12	2.35
	Return	1.08	1.13	0.96	0.95	1.11	0.43	0.49
P power	Fault	4.63	4.57	3.42	3.37	4.53	1.62	1.94
	Return	3.59	2.74	2.73	2.72	3.69	1.84	1.40
Q power	Fault	1.58	2.67	2.25	2.33	1.63	1.11	1.56
	Return	0.77	1.49	1.71	1.87	1.12	3.10	2.53
Torque	Fault	4.67	4.43	4.21	4.12	4.47	1.91	2.28
	Return	3.92	2.79	2.66	2.46	3.58	1.62	1.96
DC link	Fault	3.79	2.68	1.85	1.66	2.82	0.14	0.07
	Return	1.10	0.75	0.26	0.23	0.60	0.05	0.08

where X is the evaluated parameter such as current, voltage, active and reactive power, torque, and DC-link voltage; t_{PS} is the time point at which the corresponding fault or return period begins and t_{PE} is the time point when the corresponding period ends. A lower value of the evaluation index means better transient stability and vice versa. The evaluated stability index values for all studied cases are concentrated in Table II.

V. DISCUSSION

The simulation results of all studied parameters and cases are presented in Figs. 6-13. These parameters are compared for proposed, conventional series, parallel, series-parallel resonance, conventional bridge, and solid-state bridge FCLs.

Fig. 6 shows a comparison of the wind turbine current transient behavior under fault and return to normal periods. During the fault period $T_{FP} \in (0.25\,\text{s}, 0.31\text{s})$, the proposed FCL limits the current spike to the value of 1.23pu, which is the lowest compared to other tested FCLs. SS-FCL allows a current rise to 1.43pu, which is better than series resonance, series-parallel resonance, and parallel resonance FCLs that limit the current picks to 1.8pu, 1.87pu, and 2pu, respectively. The highest current peak of 2.04pu is obtained with B-FCL. As shown in Table II, the proposed FCL provides the best results also in the terms of transient stability with a stability index of 0.71, while the worst results of 2.15 were obtained with series resonance FCL. After the circuit breaker is tripped, the return to the normal period begins $T_{RP} \in (0.31\text{sec}, 0.4\,\text{sec})$. During this period, the transient stability of the proposed FCL was also the best with a stability index of 1.07, while series-parallel resonance, parallel resonance, and SS-FCL had almost similar stability indexes of 1.34, 1.35, and 1.35, respectively. The worst results for the return period were obtained for B-FCL, with a stability index of 1.66. It is seen from fig. 6 that the currents fluctuate for all studied FCL cases. The reason for these fluctuations is the transient response of the power system (wind turbine, FCL, and power lines) to fault disconnection by the circuit breaker. Currents for all studied cases converge (at 0.6s) together after the transient state is over. Examination of instantaneous current depicted in Fig. 7 verifies that the proposed FCL has the best current pick limitation.

The comparison of wind turbine voltage transient behavior under fault and return to normal periods is depicted in Fig. 8. For the cases where B-FCL is used and when FCL is not present in the system, the voltage drop is very deep (nearly zero). Using SS-FCL reduces the voltage drop to 0.575pu, which is the best among compared cases. The proposed FCL provides a slightly worse voltage drop of 0.515pu, while series-parallel resonance and parallel resonance FCLs result in a voltage drop of 0.17pu. Using series resonance FCL results in a voltage drop of 0.1pu. The same tendency can be seen from transient stability indexes- the SS-FCL has the best transient stability index of 2.12, while

the proposed FCL has 2.35. The worst index of 5 is obtained with B-FCL. Also during the return period, the SS-FCL has the best transient stability index of 0.43 while other tested FCLs have stability indexes between 0.49-1.11. Examination of instantaneous voltage depicted in Fig. 9 verifies that the lowest voltage drop was achieved with SS-FCL and the proposed FCL, with a slight advantage over SS-FCL.

The active power transients for all studied cases are depicted in Fig. 10. The SS-FCL limits the active power drop to 0.625pu, which is better than other FCLs. The proposed FCL limits the power drop to 0.49pu, while the series-parallel and parallel FCLs reduce active power drop to the value of 0.18pu. The series resonance FCL and B-FCL are less efficient in the reduction of active power drop and it falls almost to 0. In terms of transient stability, the SS-FCL has the best stability index of 1.62. The proposed FCL has a stability index of 1.94, series-parallel FCL has an index of 3.37, and parallel resonance FCL has an index of 3.42, while the worst index values of 4.53 and 4.57 were obtained with B-FCL and series resonance FCL, respectively. However, during the return period, the proposed FCL has the best transient stability index of 1.4, while SS-FCL has an index of 1.84. Series-parallel, parallel, and series resonance FCLs have almost the same transient stability of 2.72, 2.73, and 2.74, respectively. The worst transient stability index of 3.69 was obtained for B-FCL.

The reactive power transients for all studied cases are presented in Fig. 11. During the fault period, the SS-FCL limits the rise of reactive power to the value of 0.06pu, while the proposed FCL limits reactive power to 0.17pu. worst results of 0.69pu were obtained with series resonance FCL. The same tendency is reflected in transient stability indexes- the best stability index of 1.11 was obtained with SS-FCL, the proposed FCL has an index of 1.56 and the worst index of 2.67 was obtained for series resonance FCL. During the return period, the situation was different. The series-parallel resonance FCL has the deepest negative reactive power drop of -0.92pu. The lowest reactive power drop of -0.25 was achieved with the proposed FCL. The best transient stability index of 0.77 was achieved without FCL, while the worst index of 3.1 with SS-FCL.

The torques obtained with different FCLs are depicted in Fig. 12. During the fault period, the torque has negative sag that causes undesirable mechanical stress on the DFIG generator. The proposed and series resonant FCLs limit the torque sag to -2.05pu, while B-FCL, series-parallel, parallel and SS-FCL limit only to -2.35pu, -2.42pu, and -2.68pu respectively. The best transient stability indexes (with a slight advantage to SS-FCL) of 1.91 and 2.28 were obtained with SS-FCL and the proposed FCL, respectively. The worst transient stability index of 4.47 was obtained with B-FCL. During the return period, the situation was the same- the SS-FCL and the proposed FCL had indexes of 1.62 and 1.96, respectively. The worst transient stability index of 3.58 was obtained with B-FCL. It is important to note that SS-FCL and the proposed FCL significantly decrease torque fluctuations during both fault and return periods.

The DC-link voltages for all studied cases are depicted in Fig. 13. During the fault period, there is a spike in the DC-link voltage. The proposed FCL provided the best limitation of the voltage spike of 1.11pu while SS-FCL limited the voltage to 1.18pu. Other FCLs have significantly higher voltage spikes- 1.38pu for series-parallel resonance, 1.42pu for parallel resonance, 1.69pu for series resonance and B-FCL. The proposed FCL also has the best transient stability index of 0.07, while the worst index of 2.82 is obtained for B-FCL. During the return period, the SS-FCL and the proposed FCL have almost equal stability indexes of 0.05 and 0.08, respectively. The worst stability index of 0.6 was obtained for B-FCL.

The recovery of the current and voltage to their nominal values, which were before the fault occurrence, can be analyzed according to the speed of the recovery and fluctuations from the nominal value. The zoomed-out currents and voltages shown in Fig. 14 and 15, can be used for this analysis. It can be seen from Fig. 14 that the current in the case of the proposed FCL recovers to the nominal value at 0.5s, which is faster than for other studied cases. The current waveforms for other studied cases converge together at 0.6s and at this time point, they return to the nominal current value that was before the fault occurrence and FCL activation. The fluctuations from the nominal value are evaluated by the transient stability index. It can be seen from Table II that the transient stability evaluation index of current was the best for the proposed FCL during both fault and return periods. Therefore, the current in the case of the proposed FCL recovers faster and with smaller fluctuations than in other studied cases.

It is seen from Fig. 15 that all voltage waveforms converge together at 0.5s and they all return at 0.9s to the nominal voltage value that was before the fault occurrence and FCL activation. According to Table II, the transient stability evaluation index of the voltage for the proposed FCL case was better than other cases except for SS-FCL, which was slightly better than for the proposed FCL. Therefore, the voltage in the case of the proposed FCL recovers at the same speed as in other studied cases and with smaller fluctuations than in No FCL, SR-FCL, PR-FCL, SPR-FCL, and Bridge FCL cases. However, it has higher fluctuations than SS-FCL.

In summary, the simulation results show that during the fault period, the proposed FCL provided the best fault current spike limitation and the best transient stability of the current during fault and return periods. Furthermore, the proposed and series resonant FCLs limited the torque sag better than other studied FCLs, and the best transient stability during fault and return periods were obtained with the proposed FCL and SS-FCL. The proposed FCL also significantly decreased torque fluctuations during both fault and return periods. Furthermore, the proposed FCL provided the best limitation of the DC-link voltage spike and the best transient stability.

However, although the proposed FCL had better voltage drop limitation and transient stability than other studied resonance FCLs, the best voltage drop limitation and voltage transient stability during fault and return periods were provided by SS-FCL. The proposed FCL had better active power drop limitation and transient stability than other resonance FCLs, but the best active power drop limitation and transient stability were achieved with SS-FCL. During the return period, the best transient stability of the active power was provided by the proposed FCL. The same tendency is seen for reactive power- during the fault period, SS-FCL better limited the reactive power rise and had the best transient stability than other FCLs. However, during the return period, the best limitation of the reactive power drop was achieved with the proposed FCL.

VI. Conclusions

This paper proposes a new topology of resonance FCL based on the series resonance FCL. The proposed topology overcomes drawbacks associated with conventional resonance-based FCLs while preserving their advantages. Moreover, the proposed FCL can control the value of the limited current, like in SS-FCL. The proposed FCL can limit the fault current for the entire fault period independently of the reactor's charging state and significantly reduces the wind turbine's torque oscillations during a fault. The proposed topology was compared to B-FCL, SS-FCL, series, parallel and series-parallel resonance FCLs. All studies FCLs used inductors with internal resistance (NSFCLs). The comparison was conducted using a power system comprised of a 1.5 MW DFIG wind turbine, a 50MW synchronous generator, and two step-up transformers.

The simulation results show that during the fault period, the proposed FCL provided better transient stability and limitations of spikes and sags in most studied parameters than other tested FCLs. However, SS-FCL had better transient stability and limitation of voltage and active power drop, and reactive power rise than the proposed FCL. During the return period, the proposed FCL did not provide the best results for most of the studied parameters. Therefore, it is also important to consider the influence of the wind turbines' FCL protection during the return period.

References

[1] GWEC, Global wind report 2022, https://gwec.net/wp-content/uploads/2022/04/Annual-Wind-Report-2022_screen_final_April.pdf

[2] FS-UNEP. Global Trends in Renewable Energy Investment 2020; Technical Report; The Frankfurt School—UNEP Collaborating Centre for Climate & Sustainable Energy Finance; Frankfurt School of Finance & Management: Frankfurt, Germany, 2020.

[3] A. Bensalah, G. Barakat, and Y. Amara, "Electrical generators for large wind turbine: trends and challenges," *Energies*, vol. 15, no. 18, 6700, 2022.

[4] M. Q. Duong, S. Leva, M. Mussetta, K.H. Le, "A comparative study on controllers for improving transient stability of DFIG wind turbines during large disturbances," *Energies*, vol. 11, no. 480, 2018.

[5] J. Carroll, A. McDonald, and D. McMillan, "Reliability comparison of wind turbines with DFIG and PMG drive trains," *IEEE Transactions on Energy Conversion,* vol. 30, no. 2, pp. 663-670, 2014.

[6] D. Baimel, N.R. Chowdhury, J. Belikov, and Y. Levron, "New type of bridge fault current limiter with reduced power losses for transient stability improvement of DFIG wind farm," *Electric Power Systems Research*, vol. 197, 107293, 2021.

[7] Y. Zhang and R. A. Dougal, "State of the art of fault current limiters and their applications in smart grid," *IEEE Power and Energy Society General Meeting,* pp. 1-6, 2012.

[8] G. Pepermans, J. Driesen, D. Haeseldonckx, R. Belmans and W. D'haeseleer, "Distributed generation: definition, benefits and issues," *Energy Policy.*, vol. 33, issue 6, pp. 787-798, 2005.

[9] D. Baimel and A. Kuperman, "Full theoretical analysis with simulation-based verification of thyristors-bridge-type SFCL operation modes," *Simulation Modelling Practice and Theory*, vol. 94, 2019, pp. 349-366, 2019.

[10] J. E. T. Villas, D. Mukhedkar, V. R. Fernandes and A. C. Magalhaes, "Ground grid design of a transition station system-a typical example of fault transfer," *IEEE Transactions on Power Delivery*, vol. 5, no. 1, pp. 124-129, 1990.

[11] Z. He, J. Hu, L. Lin, Y. Chang and Z. He, "Pole-to-ground Fault Analysis for HVDC Grid Based on Common- and Differential-mode Transformation," *Journal of Modern Power Systems and Clean Energy*, vol. 8, no. 3, pp. 521-530, 2020.

[12] H.-C. Jo and S.-K. Joo, "Superconducting fault current limiter placement for power system protection using the minimax regret criterion," *IEEE Transactions on Applied Superconductivity*, vol. 25, no. 3, pp. 1-5, 2015.

[13] S. M. Blair, C. D. Booth, I. M. Elders, N. K. Singh, G. M. Burt, and J. McCarthy, "Superconducting fault current limiter application in a power-dense marine electrical system," *IET Electrical Systems in Transportation*, vol. 1, no. 3, pp. 93-102, 2011.

[14] M. T. Hagh and M. Abapour, "Nonsuperconducting fault current limiter with controlling the magnitudes of fault currents," *IEEE Transactions on Power Electronics*, vol. 24, no. 3, pp. 613-619, 2009.

[15] A. Moghadasi, A. Sarwat, J.M. Guerrero, "Multi-objective optimization in combinatorial wind farms system integration and resistive SFCL using analytical hierarchy process," *Renew. Energy*, vol. 94, pp. 366-382, 2016.

[16] Z.C. Zou, X.Y. Xiao, Y.F. Liu, Y. Zhang and Y.H. Wang, "Integrated protection of DFIG-based wind turbine with a resistive-type SFCL under symmetrical and asymmetrical faults," *IEEE Transactions on Appllied Superconductivity*, vol. 26, no. 7, pp. 1-5, 2016.

[17] J. Kozak, M. Majka, S. Kozak, and T. Janowski, "Design and tests of coreless inductive superconducting fault current limiter," *Transactions on Appllied Superconductivity*, vol. 22, no. 3, pp. 5601804-5601804, 2012.

[18] L. Jiang, J. X. Jin, and X. Y. Chen, "Fully controlled hybrid bridge type superconducting fault current limiter," *Transactions on Appllied Superconductivity*, vol. 24, no. 5, pp. 1-5, 2014.

[19] H. You and J. Jin, "Characteristic analysis of a fully controlled bridge type superconducting fault current limiter," *Transactions on Appllied Superconductivity*, vol. 26, no. 7, pp. 1-6, 2016.

[20]M. Firouzi, G.B. Gharehpetian and B. Mozafari,"Bridge-type superconducting fault current limiter effect on distance relay characteristics," *International Journal of Electrical Power & Energy Systems*, 68, 115-122, 2015.

[21] K.E. Okedu, "Enhancing DFIG wind turbine during three-phase fault using parallel interleaved converters and dynamic resistor," *IET Renew. Power Gener*, vol. 10, no. 8, pp. 1211-1219, 2016.

[22] M.S. Alam, M.A.Y. Abido, "Fault Ride Through Capability Enhancement of a Large-Scale PMSG Wind System with Bridge Type Fault Current Limiters," *Adv. Electr. Comput. Eng.*, vol. 18, no. 1, pp. 43-50, 2018.

[23] S. B. Naderi, M. Jafari and M. Tarafdar Hagh, "Parallel-Resonance-Type Fault Current Limiter," *IEEE Transactions on Industrial Electronics*, vol. 60, no. 7, pp. 2538-2546, 2013.

[24] M. R. Islam, J. Hasan, M. R. R. Shipon, M. A. H. Sadi, A. Abuhussein and T. K. Roy, "Neuro Fuzzy Logic Controlled Parallel Resonance Type Fault Current Limiter to Improve the Fault Ride Through Capability of DFIG Based Wind Farm," *IEEE Access*, vol. 8, pp. 115314-115334, 2020.

[25] M. A. H. Sadi and M. H. Ali, "Transient stability enhancement of multi-machine power system by parallel resonance type fault current limiter," *North American Power Symposium (NAPS)*, pp. 1-6, 2015.

[26] M. Farsadi, T. S. Dizaji and B. Kakesoury, "Modified parallel resonance type Fault Current Limiter," *2013 8th International Conference on Electrical and Electronics Engineering (ELECO)*, pp. 248-252, 2013.

[27] S. H. Lim, H. S. Choi, B. S. Han, "The fault current limiting characteristics of a flux-lock type high-Tc superconducting fault current limiter using series resonance, " *Cryogenics*, vol. 44, no. 4, 2004, pp. 249-254, 2004.

[28] M. M. Moghimian, M. Radmehr and M. Firouzi, "Series Resonance Fault Current Limiter (SRFCL) with MOV for LVRT Enhancement in DFIG-Based Wind Farms, " *Electric Power Components and Systems*, vol. 47, pp. 1814-1825, 2019.

[29] H. Arai, M. Inaba, T. Ishigohka, "Fundamental Characteristics of Superconducting Fault Current Limiter Using LC Resonance Circuit, " in *IEEE Transactions on Applied Superconductivity*, vol. 16, no. 2, pp. 642-645, 2006.

[30] O. Arikan, B. Kucukaydin," A new approach to limit fault current with series-parallel resonance strategy," *Electrical Engineering*, vol. 102, pp. 1287–1296, 2020.

[31] Md. Haque, Yah-Ya & Hasan, Jakir & Islam, Md. Rashidul & Islam, Md Rabiul," Low-Voltage Ride Through Capability Augmentation of DFIG-Based Wind Farms Using Series-Parallel Resonance-Type Fault Current Limiter," *Wind,* no. 1, pp. 20-43, 2021.

[32] M. Firouzi, "Low-voltage ride-through (LVRT) capability enhancement of DFIG-based wind farm by using bridge-type superconducting fault current limiter (BTSFCL)," *Journal of Power Technologies*, vol. 99, no. 4, 2020.

[33] M. S. Alam, F. S. A. Ismail, M. A. Abido, and M. A. Hossain, "Fault current limiter of VSC-HVDC systems using variable resistive bridge controller," *Ain Shams Engineering Journal*, vol. 12, no. 3, 2021.